THE JOURNAL OF PHYSICAL CHEMISTRY A

Article

pubs.acs.org/JPCA

Exploring Non-Condon Effects in a Covalent Tetracene Dimer: How Important Are Vibrations in Determining the Electronic Coupling for Singlet Fission?

Ethan C. Alguire,[‡] Joseph E. Subotnik,[‡] and Niels H. Damrauer*[,†]

[†]Department of Chemistry and Biochemistry, University of Colorado at Boulder, Boulder, Colorado 80309, United States

[‡]Department of Chemistry, University of Pennsylvania, 231 South 34th Street, Philadelphia, Pennsylvania 19104-6323, United States

Supporting Information

ABSTRACT: Singlet fission (SF) offers opportunities for wavelength-selective processing of solar photons with an end goal of achieving higher efficiency inexpensive photovoltaic or solar-fuels-producing devices. In order to evaluate new molecular design strategies and for theoretical exploration of dynamics, it is important to put in place tools for efficient calculation of the electronic coupling between single-exciton reactant and multiexciton product states. For maximum utility, the couplings should be calculated at multiple nuclear geometries (rather than assumed constant everywhere, i.e., the Condon approximation) and we must be able to evaluate couplings for covalently linked multichromophore systems. With these requirements in mind, here we discuss the simplest methodology possible for rapid calculation of diabatic one-electron coupling matrix elements—based on Boys localization and rediagonalization of molecular orbitals. We focus on a covalent species called BT1 that juxtaposes two tetracene units in a partially cofacial geometry via a norbornyl bridge. In BT1, at the equilibrium C_{2v} structure, the "nonhorizontal" couplings between HOMOs and LUMOs (t_{HL} and t_{LH}) vanish by symmetry. We then explore the impact of molecular vibrations through the calculation of t_{AB} coupling gradients along 183 normal modes of motion. Rules are established for the types of motions (irreducible representations in the C_{2v} point group) that turn on t_{HL} and t_{LH} values as well as for the patterns that emerge in constructive versus destructive interference of pathways to the SF product. For the best modes, calculated electronic coupling magnitudes for SF (at root-mean-squared deviation in position at 298 K), are within a factor of 2 of that seen for noncovalent tetracene dimers relevant to the molecular crystal. An overall "effective" electronic coupling is also given, based on the Stuchebrukhov formalism for non-Condon electron transfer rates.

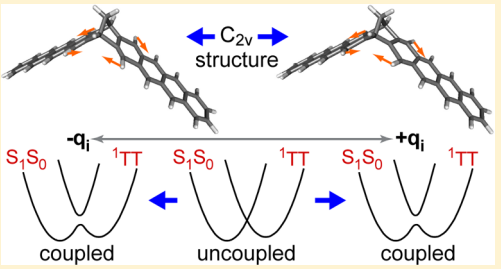

I. INTRODUCTION

Interest in achieving third-generation solar energy conversion[1]—where the ratio of efficiency versus cost would exceed that achieved in single junction crystalline and thin-film devices—has reinvigorated the exploration of organic material photophysics characterized by the fission of photoproduced singlet exciton states into singlet-coupled pairs of triplets.[2,3] This so-called singlet fission (SF) offers opportunities to process bluer solar photons into charge carriers with a quantum yield larger than 1, and properly designed devices that exploit SF may in principle exceed the Shockley−Quiesser limit[4] that bounds single junction devices.[5] While significant constraints on state energetics—where most importantly $E_{singlet} \sim 2E_{triplet}$—limit the space of available chromophores that can engage in SF, it is nonetheless the case that marked advances have occurred in recent years within several chromophore platforms that include polyacenes,[6−13] isobenzofurans,[14−17] carotenoids and polyenes,[18,19] and diimides,[20] as well as within device settings.[11,21,22] Recent advances have also occurred in theoretical treatments of SF mechanism and state energetics although important debates remain.[3,23−38] It is in this mechanistic landscape that attention is focused in this current study.

The role of nuclear conformation as well as dynamics in the process of SF remains a topic of great interest and significant discussion. Nuclear conformation is central to electronic coupling between states involved in the initial photoreaction[10,16,17,19,20,39] and arises naturally in electronic structure explorations of SF as electronic couplings can vary greatly due to orbital phase and constructive or destructive interference (that depends on nuclear geometry).[2,3,31,32,36,40−42] Dynamics have been explored directly[23−25,32,34,42−44] under the approximation that all fluctuations (modulating the energy of relevant states as well as the coupling between them) are harmonic and can be captured by a spectral density. Dynamic effects can also be inferred indirectly in electronic structure work that attempts to calculate global potential energy surfaces along relevant nuclear coordinates for states involved in the photoreaction.[30,31,33,37,45−47]

Received: October 27, 2014
Revised: December 10, 2014
Published: December 18, 2014

DOI: 10.1021/jp510777c
J. Phys. Chem. A 2015, 119, 299−311

In some systems, such as crystalline tetracene (Tc), the role of nuclear motions in the mechanism of SF, particularly the initial events following photoexcitation, remains debated despite the long history of exploration for SF. We have observed, using laser pulse shaping experiments, significant sensitivity of fission yield to low frequency intermolecular phonon modes.[48] On the one hand, these experimental observations might be partly supported by restricted-active-space (RAS) calculations by Zimmerman and co-workers, who have observed evidence for endoergic SF and a decreasing of the energy gap between the lowest energy adiabatic bright singlet exciton state and the dark multiexciton state along an intermolecular (between Tc monomers) coordinate.[33,46] Assuming that C−C stretches are also a meaningful nuclear coordinate promoting state mixing, one might then conclude that there are at least two important motions in the SF process—it is possible that fluctuations in the intermolecular coordinate are experimentally observed. On the other hand, recent electronic structure work by Yost and co-workers[27] that attempts to tie together a broad swath of experimental data suggests electronic coupling is well above k_BT at room temperature and that SF in crystalline Tc should occur in the adiabatic Marcus limit. In such a case, the dependence of electronic coupling on nuclear coordinates is weak and one might argue that one reaction coordinate is sufficient.[49−52] Finally, however, recent high level electronic structure calculations by Parker and co-workers[26] find electronic coupling between diabatic reactant and product states that is smaller than that of Yost and co-workers[27] but still significantly larger than one might expect for a low coupling limit.[50] As we will discuss briefly, although it is not the main focus of this paper, our simple methods allow for calculation of electronic coupling with good agreement with Parker and co-workers.[26] This may be useful in future calculations of dynamics in the vein of theory by Berkelbach, Hybertson, and Reichman,[23,24] and in this context, it would be interesting to take into account—via the spectral density—how phonon modes impact yields of singlet fission.

Molecular dimers for SF, which are of interest to our group, are expected to have significant sensitivity toward molecular vibration in their photoreaction rates. In very general terms, dimers present useful platforms for the study of SF mechanism[39,41,53] (a key point in this paper) but may also play an important role in future devices based on dye-sensitized solar cell technologies.[2,5] We have been interested in a series of dimers that juxtapose Tc monomer units in partially cofacial orientation via norbornyl bridges of varying size (see Figure 1 for the smallest of these). The dimers are inspired by naphthalene analogues explored by Paddon-Row and co-workers that show elegant control of exciton splitting as a function of bridge size.[54] In recent density functional theory (DFT) and time-dependent DFT (TD-DFT) computational work by our group, it was established that these systems have excited state energetic properties suitable for SF.[41] Further, the molecules[41] show, particularly the dimer BT1 with the smallest bridge, significant electronic communication between tetracene units as measured by calculation of Davydov splitting and quantification of so-called electron transfer integrals that impact splittings of canonical orbitals (highest occupied molecular orbital (HOMO) versus HOMO − 1 and lowest unoccupied molecular orbital (LUMO) versus LUMO + 1; vide infra). To achieve efficient SF, however, there are stringent demands on interchromophore electronic coupling beyond what is needed for energy or electron transfer. As we have shown previously[41] and explore more extensively in this paper, orbital symmetry arguments show us that SF pathways will vanish in the limit that certain symmetry elements of these molecules[41] are preserved.

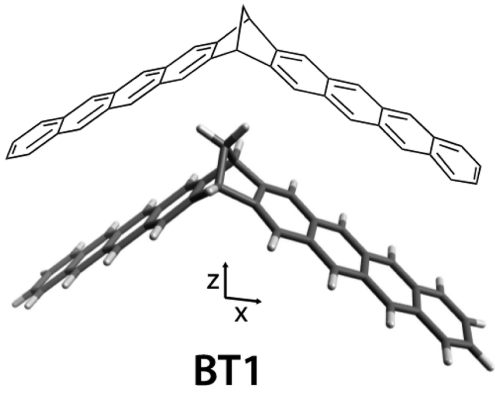

Figure 1. Two representations of the tetracene dimer BT1. The molecular structure comes from a geometry optimization calculation using the ωB97X-D density functional, the 6-31G(d) basis set, and a polarizable continuum model of solvent parametrized for toluene.[41] For the group theory analyses that follow, the molecule (C_{2v} point group) is aligned with the xz plane as shown.

The essence of this paper is to establish—with BT1 as a test case—the order of magnitude of electronic coupling for singlet fission that will arise as molecular vibrations occur and to speculate on the possibility of SF. To approach this we first establish the basis of a frontier orbital model that we will use to approximate coupling magnitudes in section II.A. In section II.B, we describe protocols for converting delocalized canonical orbitals within dimer molecules into a set of diabatic one-electron wavefunctions. These localized orbitals are in essence frontier orbitals on each chromophore of the dimer. Such functions and their couplings are essential ingredients in approximate expressions for electronic coupling between reactant and product excited states during SF. In section III.A, we first illustrate the orbital localization procedure for the case of BT1, and then establish that the couplings that arise from this description of the orbitals are comparable to those produced by Berkelbach et al. in the case of a noncovalent Tc dimer. In section III.B, we calculate gradients for these one-electronic couplings and look at projections into the directions of the normal modes of vibrational motion for BT1. Rules emerge about the types of motion (irreducible representations in C_{2v} symmetry) that permit electronic coupling necessary for SF. We then calculate the magnitude of electronic coupling that emerges during root-mean-squared (RMS) motions of the molecule at room temperature along these relevant modes. In section III.C, we give a very rough error analysis of our diabatization formalism. Finally, in section III.D, we estimate an overall effective coupling value for SF in BT1 based on Stuchebrukhov's model Hamiltonian for inelastic tunneling in a fluctuating medium. We summarize our findings and conclude in section IV.

II. THEORY

II.A. Frontier Molecular Orbital Theory for Singlet Fission. In recent electronic structure treatments of SF in class I systems, it has been common to focus on dimer structures relevant to crystalline systems and to utilize a simple frontier

DOI: 10.1021/jp510777c
J. Phys. Chem. A 2015, 119, 299−311

orbital basis set (HOMO and LUMO on each of the two chromophores A and B; referred to later as $|h_A\rangle$, $|l_A\rangle$, $|h_B\rangle$, and $|l_B\rangle$) to describe the electronic states that are involved in the nascent photoreaction within the singlet manifold, prior to dissociation and dephasing of the two triplets (see cartoon in Supporting Information, Figure S1).[2,23,24,29−32,36,42,43,53] The four-orbital basis is able to capture the essential electronic structure of five relevant diabatic states: the Frenkel exciton reactant states (S_1S_0 and S_0S_1 or superpositions of these), the charge transfer states (^{1}CA and ^{1}AC; where "A" refers to anion and "C" refers to cation), and the multiexciton product state (^{1}TT).[55] Further, the use of this basis is justified, particularly in polyacene systems, by a significant energy gap between the HOMO − 1 and lower energy occupied molecular orbitals and between the LUMO + 1 and higher energy unoccupied orbitals.[56]

The process of constructing the HOMO and LUMO for each chromophore can be accomplished by using the corresponding molecular orbitals of the chromophores as isolated molecules, as in the Hartree−Fock method described by Berkelbach, Hybertson, and Reichman (HF-BHR).[24] In bridged systems, however, obtaining a MO description of the isolated chromophores is no longer trivial. In the current paper, we instead apply a unitary transformation to the canonical MOs of the entire system to produce a localized frontier orbital representation, a process that can be equivalently applied to both intermolecular and intramolecular systems. This procedure is described in greater detail in section II.B.

In generalized rate expressions that emerge from the frontier orbital description,[2,3,24] the electronic coupling (squared) between reactants and product states (from S_1S_0 or S_0S_1 to ^{1}TT) is an essential ingredient. These states may, in principle, couple directly via a Coulomb operator; however, in many systems the matrix elements describing this are small in magnitude and "direct" pathways (see Supporting Information, Figure S1) for SF are expected to have limited mechanistic importance.[3,24,25] We will test this assumption for BT1 as described more later. An alternative route for reactant and product electronic coupling is so-called "mediated" via participation of charge transfer (CT) excited states (again see Supporting Information, Figure S1). In crystalline polyacene systems[26,27,30,31] as well as within our series of dimers,[41] the CT states are higher in energy than either the singlet exciton reactant or the ^{1}TT product. The CT states may therefore participate in coupling for SF via superexchange.[24] Berkelbach and co-workers have shown an expression for a Frenkel exciton to first order in coupling to CT states as well as for the ^{1}TT to first order in coupling to CT states.[24] From these, under the assumptions that (i) direct singlet exciton to ^{1}TT coupling (either S_1S_0 or S_0S_1 to ^{1}TT) can be ignored, (ii) $E(\mathrm{CT}) - E(S_1S_0 \text{ or } S_0S_1) \approx E(\mathrm{CT}) - E(^1\mathrm{TT}) = \Delta E_{CT}$, and (iii) we are in the nonadiabatic regime, a Marcus-like rate constant expression for conversion to $|^1\mathrm{TT}\rangle$ from a singlet exciton $|^1\mathrm{EX}\rangle$ (equal to either $|S_1S_0\rangle$ or $|S_0S_1\rangle$) can be written in the following way:[24]

$$k_{SF} \approx \frac{2\pi}{\sqrt{4\pi\hbar^2\lambda k_B T}} [|\langle {}^1\mathrm{TT}|\widehat{H}_{el}|{}^1\mathrm{CA}\rangle\langle {}^1\mathrm{CA}|\widehat{H}_{el}|{}^1\mathrm{EX}\rangle + \langle {}^1\mathrm{TT}|\widehat{H}_{el}|{}^1\mathrm{AC}\rangle \langle {}^1\mathrm{AC}|\widehat{H}_{el}|{}^1\mathrm{EX}\rangle|^2 /\Delta E_{CT}{}^2] \exp\left(\frac{-(\Delta G_{rxn} + \lambda)^2}{4\lambda k_B T}\right) \quad (1)$$

The matrix elements within the square coupling component of this rate constant may be expressed in the frontier orbital basis with one-electron off-diagonal elements of the Fock matrix and with two-electron Coulomb repulsion terms. The full expressions have been previously derived[2,23] but are shown again in Supporting Information, eq S1. For many systems described in the literature, for example crystalline polyacenes, the two-electron Coulomb terms are small and reasonably neglected.[3,24,40] We will take the same approach here and justify this approximation later in the paper. Neglecting these terms according to eq 2[2,24]

$$\begin{aligned}
\langle {}^1\mathrm{TT}|\widehat{H}_{el}|{}^1\mathrm{CA}\rangle &\approx \sqrt{3/2}\,\langle l_A|\hat{F}|h_B\rangle = \sqrt{3/2}\,t_{LH}\\
\langle {}^1\mathrm{TT}|\widehat{H}_{el}|{}^1\mathrm{AC}\rangle &\approx \sqrt{3/2}\,\langle h_A|\hat{F}|l_B\rangle = \sqrt{3/2}\,t_{HL}\\
\langle {}^1\mathrm{CA}|\widehat{H}_{el}|S_0S_1\rangle &\approx -\langle h_A|\hat{F}|h_B\rangle = -t_{HH}\\
\langle {}^1\mathrm{AC}|\widehat{H}_{el}|S_1S_0\rangle &\approx -\langle h_A|\hat{F}|h_B\rangle = -t_{HH}\\
\langle {}^1\mathrm{AC}|\widehat{H}_{el}|S_0S_1\rangle &\approx \langle l_A|\hat{F}|l_B\rangle = t_{LL}\\
\langle {}^1\mathrm{CA}|\widehat{H}_{el}|S_1S_0\rangle &\approx \langle l_A|\hat{F}|l_B\rangle = t_{LL}
\end{aligned} \quad (2)$$

expressions for electronic coupling emerge that are relevant for conversion from $|S_0S_1\rangle$ to $|^1\mathrm{TT}\rangle$ (eq 3) and from $|S_1S_0\rangle$ to $|^1\mathrm{TT}\rangle$ (eq 4).

$$\begin{aligned}
&|\langle {}^1\mathrm{TT}|\widehat{H}_{el}|{}^1\mathrm{AC}\rangle\langle {}^1\mathrm{AC}|\widehat{H}_{el}|S_0S_1\rangle\\
&\quad + \langle {}^1\mathrm{TT}|\widehat{H}_{el}|{}^1\mathrm{CA}\rangle\langle {}^1\mathrm{CA}|\widehat{H}_{el}|S_0S_1\rangle|/\Delta E_{CT}\\
&\approx |\sqrt{3/2}\,(t_{HL}t_{LL} - t_{LH}t_{HH})|/\Delta E_{CT}
\end{aligned} \quad (3)$$

$$\begin{aligned}
&|\langle {}^1\mathrm{TT}|\widehat{H}_{el}|{}^1\mathrm{CA}\rangle\langle {}^1\mathrm{CA}|\widehat{H}_{el}|S_1S_0\rangle + \langle {}^1\mathrm{TT}|\widehat{H}_{el}|{}^1\mathrm{AC}\rangle\\
&\quad \langle {}^1\mathrm{AC}|\widehat{H}_{el}|S_1S_0\rangle|/\Delta E_{CT}\\
&\approx |\sqrt{3/2}\,(t_{LH}t_{LL} - t_{HL}t_{HH})|/\Delta E_{CT}
\end{aligned} \quad (4)$$

These matrix elements will be used in what follows for comparative discussions of electronic coupling in a Tc dimer system relevant for the molecular crystal and in BT1 under conditions relevant for vibrational motion.

II.B. Computational Details: Boys Localization. All vibrational analyses and coupling element calculations employed a modified version of the Q-Chem software package,[57,58] were performed with the ωB97X-D density functional,[59] and utilized the 6-31G(d) basis set. This functional was chosen to be consistent with our previous work where we note that ωB97X-D outperforms B3LYP particularly in describing singlet excited state energies.[41] For a comparison of coupling values obtained with different functionals for two different systems (BT1 and a noncovalent Tc dimer), see the Supporting Information, Tables S3 and S4. Orbital couplings were calculated by applying Boys localization[60−62] to the HOMO − 1, ..., LUMO + 1 subspace of molecular orbitals. The resulting Boys-localized molecular

DOI: 10.1021/jp510777c
J. Phys. Chem. A 2015, 119, 299−311

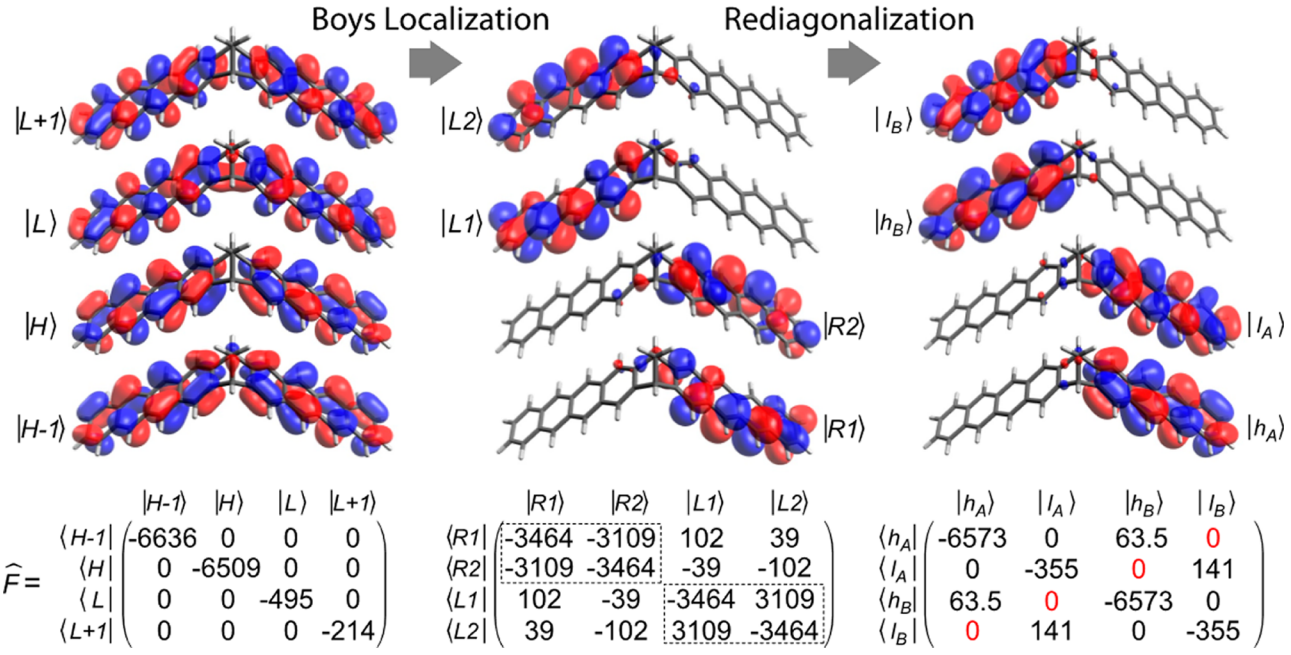

Figure 2. Localized frontier orbitals needed to calculate one-electron coupling matrix elements are obtained according to the depicted schematic. Starting with a four canonical-orbital basis set (left) consisting of two highest occupied orbitals ($|H-1\rangle$ and $|H\rangle$) and two lowest unoccupied orbitals ($|L\rangle$ and $|L+1\rangle$), Boys localization leads to four isoenergetic (in this symmetrical case) orbitals (middle), two of which are localized to the right side of the molecule ($|R1\rangle$ and $|R2\rangle$) and two of which are localized to the left ($|L1\rangle$ and $|L2\rangle$). Rediagonalization of subspaces relevant for the left and right sides of the molecule, respectively, leads (right) to the localized frontier orbitals $|h_A\rangle$, $|l_A\rangle$, $|h_B\rangle$, and $|l_B\rangle$, where "A" and "B" refer to the right and left sides of the molecule as depicted and where h and l refer to HOMO and LUMO. The representative Fock matrices for each of these three steps are also shown with the third one (right) showing orbital couplings relevant for the SF model that ignores two-electron terms. In the rightmost Fock matrix, the black zeros are a result of the diagonalization whereas the red zeros are a manifestation of the symmetry. Orbital images were generated using the free visualization tool Avogadro (version 1.1.1).[65]

orbital coefficients (C') are the result of a unitary transformation of the canonical molecular orbital subspace (C):

$$C'_{\mu p} = \sum_r C_{\mu r} U_{rp} \tag{5}$$

where the transformation matrix U is chosen such that it maximizes the Boys function (f_{Boys}), given by

$$f_{\text{Boys}}(U) = \sum_{p,q} |\langle \phi_p | \hat{X} | \phi_p \rangle - \langle \phi_q | \hat{X} | \phi_q \rangle|^2 \tag{6}$$

where $\hat{X}$ is the vectorized dipole operator and ϕ_p is the pth molecular orbital. The four resulting Boys-localized orbitals are then block diagonalized, so that the two-orbital subspaces on each chromophore are not coupled by the Fock operator. The orbitals resulting from this last transformation correspond to two HOMO/LUMO pairs, each localized to a single chromophore. Using this transformed molecular orbital basis, the Fock matrix is obtained according to

$$F'_{pq} = \sum_{\mu\nu} C'_{\mu p} F_{\mu\nu} C'_{\nu q} = \sum_{rs} U^{\mathrm{T}}_{pr} F_{rs} U_{sq} \tag{7}$$

The Coulombic repulsion terms were obtained by contracting the full atomic orbital basis two-electron integral ($\langle \mu\lambda | \nu\sigma \rangle$) with densities given by $D'^{qs}_{\lambda\sigma} = C'_{\lambda q} C'_{\sigma s}$, so that a single element of the two-electron integral tensor is obtained in the desired basis:

$$\langle pq | rs \rangle' = \sum_{\mu\nu\lambda\sigma} D'^{pr}_{\mu\nu} \langle \mu\lambda | \nu\sigma \rangle D'^{qs}_{\lambda\sigma} \tag{8}$$

It is worth emphasizing that the resulting localized MO coefficients are obtained entirely from the transformation of the canonical MO coefficients from the full-system calculation; separate calculations for isolated chromophores are not necessary. Furthermore, this approach is identical for covalent and noncovalent systems.

III. RESULTS AND DISCUSSION

III.A. Demonstrations of the Boys Method for Calculating One-Electron Coupling Matrix Elements.

III.A.1. Covalently Bridged Dimer BT1. In BT1 we take a four-orbital active space approach as described in section II.A. The starting place is four canonical Kohn–Sham orbitals for this system: $|H-1\rangle$, $|H\rangle$, $|L\rangle$, and $|L+1\rangle$. As expected, each is delocalized over the full π system of the molecule (Figure 2(left)). The energy gap from $|H-1\rangle$ to $|H-2\rangle$ (not shown) is 1280 meV, and the energy gap from $|L+1\rangle$ to $|L+2\rangle$ (not shown) is 1390 meV. It is natural to consider BT1 as being comprised of two covalently coupled Tc subunits, and from this perspective $|H-1\rangle$ and $|H\rangle$ give the appearance, respectively, of in-phase and out-of-phase superpositions of the familiar nodal pattern of the Tc monomer HOMO (see Supporting Information, Figure S2). An analogous statement can be made for $|L\rangle$ and $|L+1\rangle$ in reference to the Tc LUMO.

Also shown in Figure 2(left) is a subset of the Fock matrix inclusive of the frontier orbital basis with values reported in millielectronvolts (meV). For symmetric systems, in the limit where a one-electron Hamiltonian is accurate, one-half the energy splitting between occupied orbitals and between unoccupied orbitals is exactly equal to the electron transfer integrals T_{HT} and T_{ET}, respectively, as has been described extensively in literature focusing on donor/acceptor interactions between alkyl-separated π systems.[63,64] The quantities

DOI: 10.1021/jp510777c
J. Phys. Chem. A 2015, 119, 299–311

$|T_{HT}|$ = 63.5 meV and $|T_{ET}|$ = 141 meV are relevant for hole-transfer and electron-transfer pathways, respectively, coupling the two tetracene subunits in BT1.[41]

As discussed in the Introduction, we have sought the simplest method for calculating one-electron matrix elements describing orbital couplings *between* chromophoric subunits within dimeric molecules. To construct localized diabatic orbitals starting from the canonical frontier orbitals, we apply a unitary transformation based on Boys localization (as described in section II.B[60−62]). As can be seen in Figure 2(middle), this produces a set of four orthonormal MOs of identical energy, two of which, $|R1\rangle$ and $|R2\rangle$, are localized to the right side of BT1 and two of which, $|L1\rangle$ and $|L2\rangle$, are localized to the left side. As can be seen in the Fock matrix, there are very significant off-diagonal energy couplings between pairs of orbitals on either side of the molecule (e.g., $|\langle R1|\hat{F}|R2\rangle| = |\langle L1|\hat{F}|L2\rangle| = 3109$ meV) whereas off-diagonal couplings between left and right orbitals are small and of order 100 meV.

With these localized MOs it is now straightforward to obtain a HOMO/LUMO set for each of the chromophoric sides of the molecule by focusing on diagonalization in the two 2 × 2 subspaces that are represented by the dotted-line boxes in Figure 2(middle), as suggested in a very similar context by Cave and Newton.[66] This is achieved by the application of two Givens rotation matrices, each with a dimension NBasis × NBasis (where NBasis = 4) but each as the identity other than the 2 × 2 subspace on which it is acting. The procedure results in four new MOs as seen in Figure 2(right). For each side of the dimer (labeled "A" versus "B") a HOMO/LUMO set is generated with the expected nodal patterns relative to monomeric Tc (again, see the Supporting Information, Figure S2) and with no energy couplings between HOMO and LUMO, e.g., $\langle h_A|\hat{F}|l_A\rangle = \langle h_B|\hat{F}|l_B\rangle = 0$. Critically, however, off-diagonal matrix elements exposing energy couplings between orbitals across the dimer are permitted. As shown in the Fock matrix of Figure 2(right), $\langle h_A|\hat{F}|h_B\rangle = t_{HH} = 63.5$ meV and $\langle l_A|\hat{F}|l_B\rangle = t_{LL} = 141$ meV; both values are identical to the magnitudes $|T_{HT}|$ and $|T_{ET}|$ obtained from splittings within the canonical orbitals (vide supra). As expected from symmetry considerations, both matrix elements $\langle h_A|\hat{F}|l_B\rangle = t_{HL}$ and $\langle l_A|\hat{F}|h_B\rangle = t_{LH}$ are zero. Note that, for asymmetric systems, one cannot use HOMO/HOMO − 1 or LUMO/LUMO + 1 splittings to calculate electron transfer integrals; one is forced to use a more general approach, e.g., the Boys approach described above.

III.A.2. Digression: Noncovalent Tetracene Dimer. To quantitatively benchmark the overall procedure just described against other known methods, we have considered a noncovalent Tc dimer system where the electronic coupling for SF is expected to be large both by literature precedent[26,27,31] and by inference to a structurally and electronically related pentacene dimer for which values of t_{HH}, t_{LL}, t_{HL}, and t_{LH} have been previously reported.[24] The structure considered here (Supporting Information, Figure S3) represents one of three unique nearest neighbor pairs in the most common polymorph of crystalline Tc.[67] The choice of this dimer among the three is somewhat arbitrary as each is expected to have significant interchromophore orbital couplings, particularly the two that have the general herringbone arrangement of the Tc monomers.[24,26] We choose this structure, in part, so that comparisons can be made (vide infra) with reported high level calculations.[26] Using Hartree−Fock methods identical to those applied previously to pentacene dimers by Berkelbach, Hybertson, and Reichman (BHR-HF),[24] values were calculated for t_{HH}, t_{LL}, t_{HL}, and t_{LH}[68] and are shown in Table 1. The Boys methodology was then applied for purposes of comparison.

Table 1. Comparison of One-Electron Interchromophore Coupling Matrix Elements (in meV) and Various Products of These Elements (in meV^2) in Noncovalent Tc Dimer with Boys Method versus Previously Described Hartree−Fock Method[a]

	BHR-HF[a]	Boys
t_{HH}	−204	−91
t_{LL}	113	−83.5
t_{HL}	79	−74
t_{LH}	−88	−107
$(3/2)^{1/2}t_{LH}t_{LL}$	−12179	10942
$(3/2)^{1/2}t_{HL}t_{HH}$	−19738	8247
$(3/2)^{1/2}(t_{LH}t_{LL} - t_{HL}t_{HH})$	7559	2695
$(3/2)^{1/2}t_{HL}t_{LL}$	10933	7553
$(3/2)^{1/2}t_{LH}t_{HH}$	21987	11923
$(3/2)^{1/2}(t_{HL}t_{LL} - t_{LH}t_{HH})$	−11054	−4370

[a]Unpublished values calculated by Berkelbach[68] using previously described methods.[23,24]

The sign differences observed between the two methods originate from differing orbital phase conventions that were used. Such a sign difference is unimportant as can be seen in the various products of one-electron matrix elements (terms such as $(3/2)^{1/2}t_{HL}t_{LL}$) that are listed in Table 1: in all cases the two products whose difference is relevant for the electronic coupling (eqs 3 and 4) needed for rate expressions have a common sign indicating there will be a destructive interference between hole-transfer and electron-transfer pathways leading from the singlet exciton state to the ^{1}TT. In general there is reasonably good agreement in the magnitude of the coupling values calculated with the two methods. It is noted that, in the case of t_{HH}, the Boys method predicts a value less than half the magnitude of the HF method. This may be a manifestation of a previously noted overestimation of coupling using HF.[24,30] Along these lines, if HF exchange is used with the current Boys method instead of ωB97X-D, universally larger couplings are obtained for the Tc dimer (Supporting Information, Table S4) as well as for BT1 (Supporting Information, Table S3). We note a general increase in coupling as the extent of exact exchange is increased in the functional from PBE (where there is none), to B3LYP, to ωB97X-D, and finally to HF (which contains all exact exchange). However, it is pointed out that the magnitude of t_{HH} that we calculate for the Tc dimer with HF exchange is still approximately half that calculated by Berkelbach.[68] It is noted that a factor of 2 discrepancy between couplings from single molecule and supramolecular calculations has been seen previously for excitonic couplings.[69]

It is worthwhile to consider some measure of electronic coupling between diabatic states involved in SF in order to connect to other theoretical treatments in the literature. As discussed in section II, quantities such as $|(3/2)^{1/2}(t_{HL}t_{LL} - t_{LH}t_{HH})|$ and $|(3/2)^{1/2}(t_{LH}t_{LL} - t_{HL}t_{HH})|$ serve as useful approximations to relevant superpositions of superexchange coupling pathways in SF from either S_0S_1 (eq 3) or S_1S_0 (eq 4), respectively. We highlight in Table 1 the quantity $(3/2)^{1/2}(t_{HL}t_{LL} - t_{LH}t_{HH})$ relevant for $S_0S_1 \rightarrow {}^1$TT (eq 3) as opposed to $(3/2)^{1/2}(t_{LH}t_{LL} - t_{HL}t_{HH})$ relevant for $S_1S_0 \rightarrow {}^1$TT (eq 4) as the magnitude is larger for the former quantity using both methods. With the Boys method, $|(3/2)^{1/2}(t_{HL}t_{LL} -$

DOI: 10.1021/jp510777c
J. Phys. Chem. A 2015, 119, 299−311

$t_{LH}t_{HH}$)| = 4370 meV^2. This is within 30% of values extracted from diabatic state couplings obtained in a high level calculation of a model Hamiltonian for a tetracene dimer by Parker and Shiozaki[26] where

$$|\langle {}^1\mathrm{TT}|\widehat{H}_{el}|{}^1\mathrm{AC}\rangle\langle {}^1\mathrm{AC}|\widehat{H}_{el}|S_0S_1\rangle + \langle {}^1\mathrm{TT}|\widehat{H}_{el}|{}^1\mathrm{CA}\rangle \langle {}^1\mathrm{CA}|\widehat{H}_{el}|S_0S_1\rangle| = 3233\ \mathrm{meV}^2$$

Working backward from the individual state coupling matrix elements in this model Hamiltonian, again under the assumption that Coulomb terms due to two-electron overlap densities are small, it is possible to extract one-electron terms where t_{HH} = 100 meV, t_{LL} = 88 meV, t_{HL} = 45 meV, and t_{LH} = 66 meV. These are also in reasonably good agreement with values obtained by the simpler methods listed in Table 1.

Before leaving this model noncovalent dimer and returning to discussions of BT1, we note that all methods discussed in this section—Parker/Shiozaki, Boys, BHR-HF (in order of increasing value)—predict, under a superexchange model, a magnitude of electronic coupling in SF that is less than k_BT (298 K) ranging from 3 to 11 meV (ours is 4.4 meV) when using ΔE_{CT} = 1000 meV as per the high-level calculations by Parker and Shiozaki of a Tc dimer imbedded in a point-charge "supercell" to mimic aspects of the crystalline environment.[26] It should be pointed out that even the most accurate Parker/Shiozaki model cannot accommodate charge delocalization or polarization of the crystal environment to the new charge distribution, and as such the estimate of ΔE_{CT} may still be too high. Electroabsorption studies suggest the CT states to be in the range 2.7−3.1 eV,[70] suggesting ΔE_{CT} in a range of 400−800 meV above the singlet exciton state of 2.32 eV.[71] If we choose for purposes of comparison the median case of ΔE_{CT} = 600 meV, the range of electronic couplings being discussed shifts to 5−18 meV with our prediction using the Boys methodology at 7.3 meV. Although shifted to higher values, the individual values within this range remain less than k_BT and notably less than recent calculations (varying values of ΔE_{CT}).[27,31] Further investigation will be needed to ascertain the source of this discrepancy.

III.B. Coupling Gradients and the Role of Vibrations. We now return to the BT1 dimer. The matrix elements t_{HL} and t_{LH} are calculated to be zero for the molecule in its ground state structure with C_{2v} point group symmetry. This is the expected result obtained by invoking the Longuet−Higgins−Roberts[43,72] (or Mulliken[73,74]) approximation stating that matrix elements of the type $\langle\varphi_A|\hat{F}|\varphi_B\rangle$ are proportional to the overlap integral $\langle\varphi_A|\varphi_B\rangle$. Here, orbital symmetry arguments are useful in that either localized HOMO orbital h_A or h_B is antisymmetric with respect to a reflection plane passing through both Tc units, while either LUMO l_A or l_B is symmetric. Thus, HOMO/LUMO overlaps (from A to B or from B to A) must be zero. It stands to reason, then, that certain molecular vibrations, specifically those that break the plane of symmetry in the molecule, should impact electronic coupling through nonzero values of t_{HL} and t_{LH}. To explore this, we have calculated gradients dt/dq_i for all of the interchromophore orbital couplings t_{HH}, t_{LL}, t_{HL}, and t_{LH}, where q_i refers to each of the 183 normal modes of motion for BT1. Each gradient was calculated by performing a finite difference calculation according to eq 9

$$\frac{dt}{dq_i} \approx \frac{t(\mathbf{r}_0 + \mathbf{h}_i) - t(\mathbf{r}_0 - \mathbf{h}_i)}{2|\mathbf{h}_i|} \quad (9)$$

where $\mathbf{r}_0$ is the reference geometry, and $\mathbf{h}_i$ represents a geometric perturbation in the direction of normal mode q_i, with $|\mathbf{h}_i|$ = 0.0001 Å. This value for $|\mathbf{h}_i|$ was found to be the best-converged step size for finite difference coupling gradient calculations; selected gradients for different values of $|\mathbf{h}_i|$ can be found in the Supporting Information, Table S5. A separate calculation was needed to generate the couplings for each perturbed geometry, so the total number of single point calculations necessary to approximate the coupling gradients was 366.

Certain patterns emerge in these calculated coupling gradients (all values are listed in the Supporting Information, Table S1) that can be linked to the irreducible representations of the C_{2v} point group assigned to each normal mode of motion. Examples are illustrated in Figure 3, where coupling

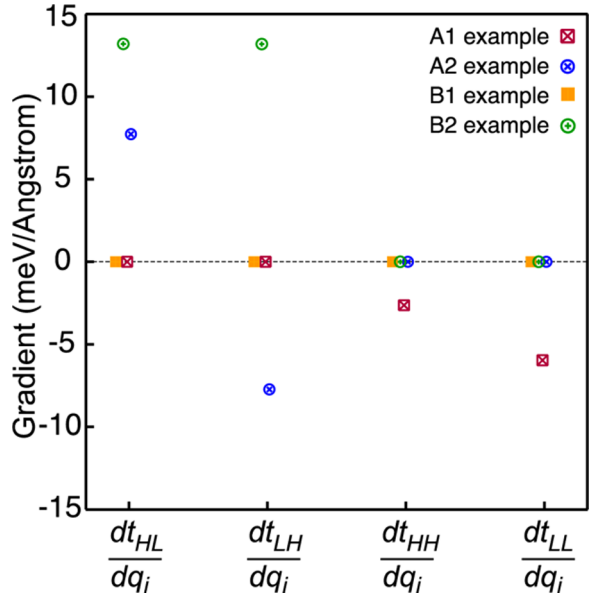

Figure 3. Examples of patterns in the one-electron coupling gradients (in meV/Å) for each type of vibrational mode according to its irreducible representation (A_1, A_2, B_1, and B_2; relevant for the C_{2v} point group symmetry of the molecule). Those shown correspond to the lowest-frequency instances of each: A_1 at 21 cm^{-1}, A_2 at 81 cm^{-1}, B_1 at 44 cm^{-1}, and B_2 at 72 cm^{-1}. Of note, only A_2 and B_2 modes have nonzero values for dt_{HL}/dq_i and dt_{LH}/dq_i. In all B_2 modes these have the same sign, whereas in all A_2 modes these have opposite signs.

gradients for the lowest frequency A_1, A_2, B_1, and B_2 modes are shown. For purposes of assignment, it is assumed that the C_2 symmetry axis of the molecule is aligned with the Cartesian z-axis, that the Cartesian xz plane bisects the molecule through both Tc units of the dimer, and that the function x transforms as the irreducible representation B_1. For all B_1 modes, *all* coupling gradients are zero. For all A_1 modes, the gradients dt_{HH}/dq_i and dt_{LL}/dq_i are finite with different magnitudes (either can be either sign) but these are ultimately irrelevant in the context of SF because dt_{HL}/dq_i and dt_{LH}/dq_i = 0. This latter point is the expected result because normal motions classified with the A_1 irreducible representation (and with B_1 as well) are symmetrical with respect to symmetry operation of reflection through the xz plane ($\hat{\sigma}_{xz}$) and cannot facilitate coupling

DOI: 10.1021/jp510777c
J. Phys. Chem. A 2015, 119, 299−311

between antisymmetrical HOMOs with symmetrical LUMOs. Thus, these results suggest A_1 and B_1 vibrations play no role in SF for BT1.

This leaves motions belonging to the A_2 and B_2 irreducible representations. Both induce no change in coupling between HOMOs or between LUMOs of the two chromophoric units of the molecule; i.e., dt_{HH}/dq_i and $dt_{LL}/dq_i = 0$. More importantly, the HOMO/LUMO coupling gradients dt_{HL}/dq_i and dt_{LH}/dq_i are nonzero. In the case of all B_2 modes, both gradients are of equal magnitude and equal sign (but can be either positive or negative). In the case of all A_2 modes, both gradients are again of equal magnitude but take on opposite signs. It is noted that the absolute sign for any of these coupling gradients for either A_2 or B_2 modes is somewhat arbitrary as it will flip in the $-q_i$ direction. However, as discussed below, the sign difference between dt_{HL}/dq_i and dt_{LH}/dq_i for A_2 modes compared to its similarity in B_2 modes *is* important.

As noted above, all coupling gradients are listed in the Supporting Information, Table S1, but for illustrative purposes, we plot just dt_{LH}/dq_i in Figure 4. Of note, there is a single B_2

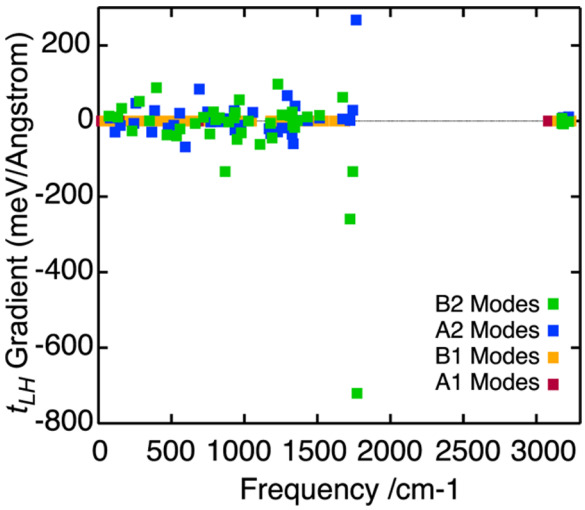

Figure 4. Coupling gradient dt_{LH}/dq shown for all frequencies and according to the irreducible representation of each mode: A_1 (red), A_2 (blue), B_1 (orange), and B_2 (green). For each frequency the corresponding gradient dt_{HL}/dq can be inferred using the pattern according to Figure 3.

normal mode at 1772 cm^{-1} (mode no. 159) that is dominant in its impact on dt_{LH}/dq (and by inference dt_{HL}/dq) relative to other modes. In terms of the magnitude $|dt_{LH}/dq|$, its value of 721 meV/Å is a factor of 2.7 larger than the next largest (267 meV/Å) occurring at 1765 cm^{-1} for an A_2 mode (mode no. 158).

In Figure 5a is plotted a cartoon of this normal mode (no. 159) with projection vectors as well as an exaggerated view of the molecule at its vibrational turning points. The perspective in these pictures is in the positive z direction with the central methylene group at the apex of the molecule in the background. The impact on electronic coupling between the Tc chromophores in the dimer is clearly a result of distortions derived from C−C stretching localized significantly to the norbornyl bridging unit and nearest phenyl rings where through-bond and through-space interactions between l_A and h_B (or vice versa) are largest. Focusing on through-space interactions, a qualitative explanation is provided that focuses

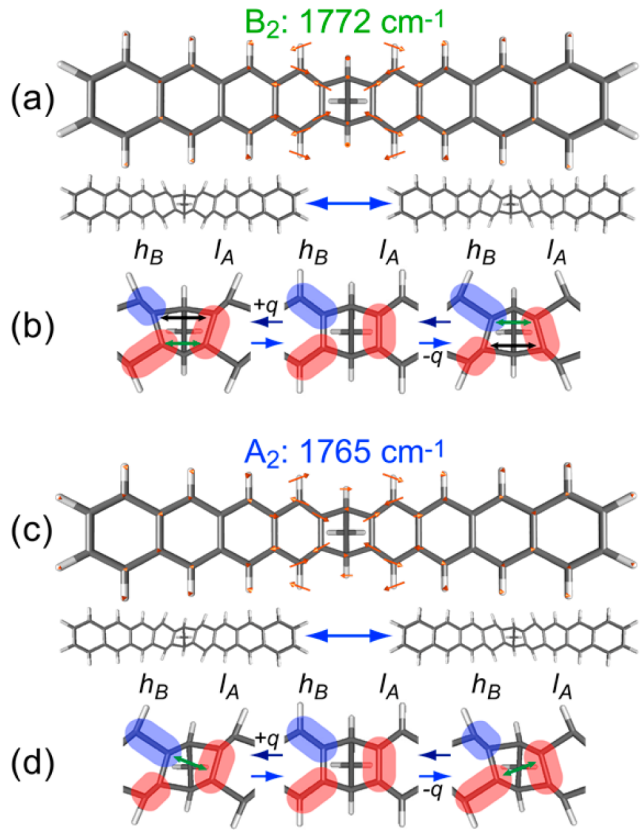

Figure 5. (a) Depiction of 1772 cm^{-1} B_2 normal mode of motion (no. 159) that has the highest magnitude coupling gradient dt_{LH}/dq. The viewpoint is in the $+z$ direction such that the central methylene group of the molecule is headed into the paper. (b) Cartoon rationalizing how t_{LH} coupling develops during this motion (in both $+q$ and $-q$ directions) with the focus on only part of the orbital (phase inferred from Figure 2) for l_A and h_B (see text for details). (c) Depiction of A_2 1765 cm^{-1} normal mode of motion (no. 158) that has the second highest magnitude coupling gradient dt_{LH}/dq. (d) Cartoon rationalizing how t_{LH} coupling develops during this motion (in both $+q$ and $-q$ directions) with the focus on only part of the orbital for l_A and h_B (again, see text for details).

on only a piece of the orbital phase for l_A and h_B at the norbornyl bridge with phase information inferred from Figure 2(right). In the center of Figure 5b the molecule is captured in its static C_{2v} structure where, by the symmetry arguments described above, there is no net overlap between l_A and h_B and t_{LH} is zero. Using an exaggerated distortion in this B_2 direction (left), it is shown that interorbital energy coupling can develop as inferred by an increase in overlap (green double arrow) of regions of l_A and h_B that are in-phase concomitant with a decrease (black double arrow) of out-of-phase overlap. In the $-q$ direction (right) a similar process happens but it results—due to phase—in a coupling matrix element of opposite sign. As shown in the Supporting Information, Figure S4b, an analogous qualitative argument applied to h_A and l_B (as opposed to l_A and h_B as discussed above) explains how dt_{HL}/dq_i and dt_{LH}/dq_i have the same sign for B_2 motions.

The A_2 mode (1765 cm^{-1}; no. 158) that has the second largest magnitude of coupling gradient dt_{LH}/dq_i (and again by inference dt_{HL}/dq_i) also involves distortions largely localized to the norbornyl bridge and nearest phenyl rings (Figure 5c). Here it can be seen that interorbital coupling can develop as the vibration proceeds as inferred from l_A to h_B orbital overlap

DOI: 10.1021/jp510777c
J. Phys. Chem. A 2015, 119, 299−311

diagonally across the bridge (Figure 5d). The magnitude of the coupling gradient dt_{LH}/dq_i in this case is understandably smaller (the factor of 2.7 mentioned above) than the 1772 cm^{-1} B_2 mode (no. 159) where coupling develops via l_A to h_B π overlap directly across the bridge.

In order to calculate coupling values as opposed to coupling gradients—given that t_{LH} (and t_{HL}) equal 0 for the static C_{2v} structure—we rely on an estimation of the deviation in position that may be expected to occur at a given temperature for any of the normal modes of motion q_i. With eq 10, an average vibrational level occupation number $\langle n_i \rangle$ is first calculated (for what follows, 298 K is used). With this, the root-mean-squared (RMS) deviation in the q_i^{th} direction ($\langle q_i^2 \rangle^{1/2}$) is then evaluated using eq 11. In these equations, ω_i and μ_i refer to the frequency and reduced mass of the ith normal mode. Finally, we calculate coupling at this RMS deviation using eq 12. These data are compiled in the Supporting Information, Table S2.

$$\langle n_i \rangle = \frac{1}{e^{\hbar\omega_i/k_B T} - 1} \tag{10}$$

$$\sqrt{\langle q_i^2 \rangle} = \sqrt{\frac{\hbar}{2\mu_i\omega_i}(2\langle n_i \rangle + 1)} \tag{11}$$

$$\Delta t_{AB} = \frac{dt_{AB}}{dq_i}\sqrt{\langle q_i^2 \rangle} \tag{12}$$

Given the relatively high frequency of the two modes discussed above (1772 and 1765 cm^{-1}), the average occupation number $\langle n \rangle$ at room temperature is 0.00, i.e., the vibrational ground state. This leads to a 0.035 Å RMS deviation for both modes and coupling values ($t_{LH} + \Delta t_{LH}$) equal to 9.45 meV (1765 cm^{-1}; A_2) and −25 meV (1772 cm^{-1}; B_2). While the magnitudes of these coupling contributions vary substantially, their impact on SF is expected to be quite similar by coincidence. This originates in the difference of terms (products of one-electron matrix elements) central to the electronic coupling expressions in eqs 3 and 4 (e.g., $t_{HL}t_{LL} - t_{LH}t_{HH}$). As seen in the Fock matrix following localization and rediagonalization in Figure 2(right), the quantities t_{HH} and t_{LL} have a common sign for this molecular system. This confluence means that A_2 modes, where there is a sign difference between Δt_{LH} and Δt_{HL} (Supporting Information, Table S2), will fare better due to a constructive interference of pathways than B_2 modes where Δt_{LH} and Δt_{HL} have a common sign. That the B_2 modes have any role in SF relies on the fact that the hole-transfer and electron-transfer pathways for donor−acceptor interactions between the two chromophores (i.e., t_{HH} and t_{LL}) have differing importance in this system (vide supra).[41] Using the value of ΔE_{CT} = 659 meV determined previously by our group for BT1,[41] we calculate the coupling relevant for rate expressions such as eq 1 according to either eq 13 ($S_0S_1 \rightarrow {}^1TT$) or eq 14 ($S_1S_0 \rightarrow {}^1TT$) and find a remarkably similar 3.589 meV for the A_2 mode (1765 cm^{-1}; no. 158) versus 3.594 meV for the B_2 mode (1772 cm^{-1}; no. 158). In this system, electronic coupling for either $S_0S_1 \rightarrow {}^1TT$ or $S_1S_0 \rightarrow {}^1TT$ is identical because in all cases (modes) $|t_{HL}| = |t_{LH}|$.

$$\text{coupling}_{(S_0S_1 \rightarrow {}^1TT)} = |[\sqrt{3/2}\,(t_{HL} + \Delta t_{HL})(t_{LL} + \Delta t_{LL}) - \sqrt{3/2}\,(t_{LH} + \Delta t_{LH})(t_{HH} + \Delta t_{HH})]/\Delta E_{CT}| \tag{13}$$

$$\text{coupling}_{(S_1S_0 \rightarrow {}^1TT)} = |[\sqrt{3/2}\,(t_{LH} + \Delta t_{LH})(t_{LL} + \Delta t_{LL}) - \sqrt{3/2}\,(t_{HL} + \Delta t_{HL})(t_{HH} + \Delta t_{HH})]/\Delta E_{CT}| \tag{14}$$

The identical procedure applied to all modes results in a set of coupling values shown in Figure 6 and listed in the Supporting Information, Table S2. In general, it can be seen that A_2 modes feature prominently as may be expected from the pathway interference issues discussed above.

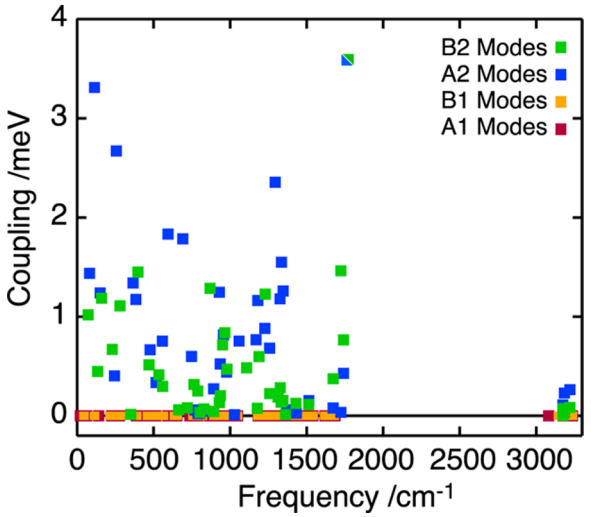

Figure 6. Electronic coupling (S_0S_1 to ^1TT; mediated via virtual CT states) calculated (eq 13) at RMS deviation in position (298 K) for each normal mode and plotted as a function of frequency and according to irreducible representation (A_1 (red), A_2 (blue), B_1 (orange), and B_2 (green)). The value for ΔE_{CT} is 659 meV as determined in previous work by our group.[41]

Of these, the 113.5 cm^{-1} vibration (no. 6) is notable with a coupling value of 3.31 meV ranking it third among all modes and 92% of the maximum at 3.59 meV. While the gradient magnitude for this mode $|dt_{LH}/dq|$ (or $|dt_{HL}/dq|$) is not insignificant, it nonetheless ranks 11th among A_2 modes and 28th overall. The significant coupling arises in large part due to its low frequency, which permits an average population of higher quantum states and with that a larger RMS deviation in position. Here, via eq 10, $\langle n \rangle$ = 1.37, to be compared with the $\langle n \rangle$ = 0.00 described above for the 1772 and 1765 cm^{-1} modes, and to $\langle n \rangle$ = 0.41 for a more modestly higher frequency 257 cm^{-1} A_2 mode (no. 16). The resulting RMS deviation (eq 11) for the 113.5 cm^{-1} vibration is $\langle q^2 \rangle^{1/2}$ = 0.30 Å, making it nearly an order of magnitude larger than the 1772 and 1765 cm^{-1} vibrations (vide supra) and twice as large as the 257 cm^{-1} A_2 mode where $\langle q^2 \rangle^{1/2}$ = 0.15 Å.

III.C. Evaluation of the Two-Electron Coupling Contribution. As has been discussed, the electronic coupling for mediated SF evaluated using either eq 13 or 14 ignores two-electron repulsion integrals that are, for example, shown in the Supporting Information, eq S1. Although these integrals are time-consuming to numerically evaluate, we have considered several cases for purposes of comparison. First, within the Supporting Information, eq S1, all integrals (two-electron or one-electron) associated with the terms $\langle {}^1TT|\widehat{H}_{el}|{}^1CA\rangle$ or $\langle {}^1TT|\widehat{H}_{el}|{}^1AC\rangle$ vanish with C_{2v} symmetry. We consider, then,

DOI: 10.1021/jp510777c
J. Phys. Chem. A 2015, 119, 299−311

four cases involving RMS deviation along two high-frequency modes (nos. 158 and 159: 1765 cm^{-1} (A_2) and 1772 cm^{-1} (B_2)) and along two low-frequency modes (nos. 4 and 6: 72 cm^{-1} (B_2) and 113.5 cm^{-1} (A_2)). Expressions inclusive of two-electron integral terms that are analogous to eqs 13 and 14 are shown in the Supporting Information, eqs S2 and S3. Because of symmetry, only one of these needs to be evaluated and we have considered the integrals relevant for the Supporting Information, eq S3 (i.e., for $S_1S_0 \rightarrow {}^1TT$). We find relatively small deviations in couplings calculated with or without the two-electron integrals. For the 1772 cm^{-1} B_2 mode, the magnitude of coupling is calculated to be 3.81 meV (including two-electron integrals) as compared with 3.59 meV (one-electron integrals), representing a very modest 6% difference. Similarly for the 1765 cm^{-1} A_2 mode, we find a 6.5% difference (3.84 meV (two-electron) versus 3.589 (one-electron)). For the lower frequency modes we find slightly larger, although still small, deviations. At 72 cm^{-1} (B_2) the relative error is 8% (0.95 meV (two-electron) versus 1.03 meV (one-electron)) while at 113.5 cm^{-1} the relative error is 11% (2.98 meV (two-electron) versus 3.31 meV (one-electron)). These results, while not complete for all A_2 and B_2 modes, nonetheless appear to justify using the simpler one-electron coupling expressions (eqs 13 and 14) particularly in computationally expensive scenarios such as during explorations of dynamics.

For completeness we have also considered the magnitude of electronic coupling for direct S_1S_0 (or S_0S_1) $\rightarrow {}^1TT$ SF, which as described earlier also depends on two-electron repulsion integrals. In the frontier orbital basis, the direct electronic coupling matrix element $\langle {}^1TT|\widehat{H}_{el}|S_1S_0\rangle$ (or $\langle {}^1TT|\widehat{H}_{el}|S_0S_1\rangle$) is given as a difference between two two-electron integrals[2,23,75] (see the Supporting Information, eq S1) that also vanish with the C_{2v} symmetry of this system. Evaluation of these integrals at RMS deviation along the four modes discussed above leads to direct electronic coupling magnitudes that are less than 1 meV just as is seen in crystalline pentacene.[24] To be precise, the exact magnitudes we calculate—that would augment the mediated couplings discussed above—are 0.37 meV (no. 4; 72 cm^{-1}; B_2), 0.37 meV (no. 6; 113.5 cm^{-1}; A_2), 0.60 meV (no. 158; 1765 cm^{-1}; A_2), and 0.50 meV (no. 159; 1772 cm^{-1}; B_2). For modes 6, 158, and 159—where coupling for mediated SF is significant at RMS deviation in position—ignoring the direct mechanism amounts to underestimating coupling with a small error of order 12%. For the lower frequency B_2 mode (no. 4; 72 cm^{-1})—where the mediated coupling magnitude is small (1.03 meV; one-electron terms)—the error incurred is modestly larger and of order 26%. It can be inferred from these sets of calculations that one-electron terms do a reasonable job capturing the magnitude of the electronic coupling for SF in this system.

III.D. Calculation of the SF Rate and Effective Total Coupling. Our final goal in this paper is to calculate an overall effective singlet fission coupling value by applying the procedure proposed by Stuchebrukhov et al.[76] for determining the rate of inelastic tunneling in a fluctuating medium. Under this model, we consider BT1 a two-level system weakly coupled to a bath of harmonic oscillators (i.e., its vibrational modes), with the model Hamiltonian given by eq 15.

$$\hat{H} = E_{S_1}|S_1S_0\rangle\langle S_1S_0| + E_{^1TT}|{}^1TT\rangle\langle {}^1TT| + \sum_{\alpha}\left[c_\alpha\hat{\sigma}_x + \sum_{i=S_1,{}^1TT} g_{i,\alpha}|i\rangle\langle i|\right](\hat{a}_\alpha^\dagger + \hat{a}_\alpha) + \frac{1}{2}\hbar\omega_\alpha\hat{a}_\alpha^\dagger a_\alpha \tag{15}$$

In this expression, $\hat{a}_\alpha^\dagger$ and $\hat{a}_\alpha$ are creation and annihilation operators of bath mode α, $g_{i,\alpha}$ is proportional to the energy gradient of electronic state i with respect to mode α, $g_{i,\alpha} = (\hbar/(2m_\alpha\omega_\alpha))^{1/2}(\partial E_i/\partial q_\alpha)$ and $\hat{\sigma}_x = |S_1S_0\rangle\langle {}^1TT| + |{}^1TT\rangle\langle S_1S_0|$. Critical to eq 15 in terms of the general findings of this work is the term c_α, which is proportional to the electronic coupling gradient with respect to mode α. The c_α term is determined using eq 16 , for which we use $\Delta E_{CT} = 659$ meV.[41]

$$c_\alpha = \sqrt{\frac{3\hbar}{4m_\alpha\omega_\alpha}}\left[\left(\frac{dt_{HL}}{dq_\alpha}\right)t_{LL} + t_{HL}\left(\frac{dt_{LL}}{dq_\alpha}\right) - \left(\frac{dt_{LH}}{dq_\alpha}\right)t_{HH} - t_{LH}\left(\frac{dt_{HH}}{dq_\alpha}\right)\right](\Delta E_{CT})^{-1} \tag{16}$$

Due to molecular orbital symmetry, to first order, the normal modes of BT1 either change the energy of the frontier orbitals (A_1 and B_1 modes) or the coupling between them (A_2 and B_2 modes), but not both (see Table S6). Thus, for a given mode, either $c_\alpha \neq 0$ or $g_\alpha \neq 0$, but never both. To clarify the distinction, from this point on A_2 and B_2 modes will only be indexed by α, while A_1 and B_1 modes will only be indexed by β.

For the spin-boson-like Hamiltonian in eq 15, following Stuchebrukhov et al.,[76] we solve for the golden rule rate, making the following substitution and assumptions. First, the reorganization energy (λ) of the SF reaction is given by the following expression:

$$\lambda = \sum_{\beta}\frac{(g_{^1TT,\beta} - g_{S_1S_0,\beta})^2}{\hbar\omega_\beta} \tag{17}$$

Second, we assume we are in the Marcus nonadiabatic limit, in which the effective coupling is the smallest parameter in the Hamiltonian. It has been suggested that similar systems may actually fall within the adiabatic Marcus limit[27] or the Redfield limit.[23,24]

Third, the system is taken to be in the thermal activation limit where eq 18 holds.

$$\sum_{\beta}(g_{^1TT,\beta} - g_{S_1S_0,\beta})^2\frac{\langle n_\beta\rangle}{(\hbar\omega_\beta)^2} \gg 1 \tag{18}$$

Fourth, the A_1 and B_1 modes are assumed to be in the classical limit, so that $\langle n_\beta\rangle = k_BT/\hbar\omega_\beta$. This fourth assumption is a weak requirement compared to the second and third assumptions, and can be generalized easily. With these assumptions, the resulting rate expression is given by eq 19. For the purposes of our calculations, we take $E_{^1TT} - E_{S_1S_0}$ to be 30 meV.[41]

DOI: 10.1021/jp510777c
J. Phys. Chem. A 2015, 119, 299−311

$$k_{^1\mathrm{TT}\leftarrow \mathrm{S_1S_0}} = \frac{1}{\hbar}\sqrt{\frac{\pi}{k_\mathrm{B}T\lambda}}\sum_\alpha c_\alpha{}^2\left[\langle n_\alpha\rangle \exp\left(-\frac{(E_{^1\mathrm{TT}} - E_{\mathrm{S_1S_0}} + \hbar\omega_\alpha - \lambda)^2}{4k_\mathrm{B}T\lambda}\right) + (\langle n_\alpha\rangle + 1)\exp\left(-\frac{(E_{^1\mathrm{TT}} - E_{\mathrm{S_1S_0}} - \hbar\omega_\alpha - \lambda)^2}{4k_\mathrm{B}T\lambda}\right)\right] \quad (19)$$

The rate constant (k) obtained from eq 19 can then be used as a parameter in the classical-limit Marcus nonadiabatic rate equation (eq 20) to solve for the effective total coupling V_{eff} as a function of the reorganization energy. The resulting possible values for V_{eff} are shown in Figure 7.

$$k_{^1\mathrm{TT}\leftarrow \mathrm{S_1S_0}} = \frac{|V_{eff}|^2}{\hbar}\sqrt{\frac{\pi}{k_\mathrm{B}T\lambda}}\exp\left(-\frac{(E_{^1\mathrm{TT}} - E_{\mathrm{S_1S_0}} - \lambda)^2}{4k_\mathrm{B}T\lambda}\right) \quad (20)$$

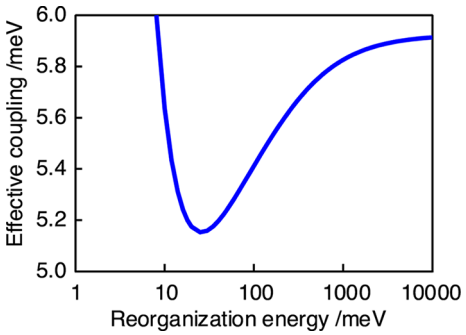

Figure 7. Effective SF coupling in BT1 for a range of reorganization energies as determined by the Stuchebrukhov formalism, for which we equate eq 19 with eq 20 and solve for $|V_{eff}|$, using $E^1_{\mathrm{TT}} - E_{\mathrm{S_1S_0}} = 30$ meV and $\Delta E_{\mathrm{CT}} = 659$ meV.[41] The SF coupling terms c_α are inversely proportional to ΔE_{CT} within the frontier orbital model (cf. eq 16).

According to Figure 7, we are able to calculate an effective coupling for BT1 for a range of reorganization energies. For large enough λ, the effective coupling approaches 5.9 meV, but is never smaller than 5.1 meV. For small reorganization energy, we note that our coupling estimate is less reliable, as the assumption of the thermal activation limit is no longer valid. However, under the assumptions detailed here, our results show a robust coupling of 5−6 meV.[25,77]

Interestingly, it is clear from Figure 7 that the effective coupling $|V_{eff}|$ converges as λ becomes large. In the limit where $\lambda \gg |E^1_{\mathrm{TT}} - E_{\mathrm{S_1S_0}}|$, the square of the effective coupling becomes simply a weighted sum of the squares of the vibrationally induced couplings (eq 21).

$$|V_{eff}|^2 = \sum_\alpha c_\alpha{}^2\,\mathrm{csch}\left(\frac{\hbar\omega_\alpha}{2k_\mathrm{B}T}\right) \quad (21)$$

It would be interesting to investigate $|V_{eff}|$ for other cases where zero diabatic coupling for SF is expected for static structures such as in facially stacked pentacene[37] or in other symmetrical covalent dimer systems.[3,39]

IV. CONCLUSIONS

The search for new molecular and material platforms for SF demands inexpensive but effective computational tools that not only predict state energetics but also allow for facile exploration of key sources of electronic coupling in this multielectron photoreaction including the role played by intra- and intermolecular vibrations. In this current work we have discussed the simplest approach possible to calculate couplings between diabatic one-electron wavefunctions localized to chromophores within intramolecular or intermolecular dimeric systems. These couplings are critical ingredients in approximate theoretical treatments of SF mediated by virtual charge transfer states.

In summary, one starts with the relevant subset of canonical (adiabatic) molecular orbitals (here, HOMO − 1··· LUMO + 1) accessed through a typical electronic structure calculation such as DFT. Application of a unitary transformation based on the localization scheme of Boys leads to pairs of orbitals that separately occupy space on each of the two chromophores A and B of the dimer. A rediagonalization procedure[66] reveals the HOMO/LUMO pair localized to each of the two chromophores A and B as well as the desired diabatic couplings t_{AB}: t_{HH}, t_{LL}, t_{HL}, and t_{LH}. This procedure avoids reliance on more expensive multireference calculations, has zero marginal cost relative to a DFT calculation, is entirely black box, and can be applied to covalently or noncovalently linked systems. The method was tested first on a dimer of Tc monomers in a geometry relevant for the molecular crystal. The calculated t_{AB} couplings are in good agreement with those inferred from reported high level calculations,[26] and those determined using the methods of Berkelbach and co-workers.[23,24,68]

We now turn to the main system focus of this paper: the norbornyl-bridged tetracene dimer BT1.[41] In the ground state optimized geometry (C_{2v} point group), the elements t_{LH} and t_{HL}, that are essential for mediated SF, vanish by symmetry. This suggests value in considering the role played by molecular vibrations that can impact molecular symmetry. In this vein, we calculated the coupling gradients dt_{HH}/dq_i, dt_{LL}/dq_i, dt_{HL}/dq_i, and dt_{LH}/dq_i for all 183 normal modes of motion.

On the one hand, we find that, for motions transforming as the A_1 or B_1 irreducible representations, the "nonhorizontal" terms t_{HL} and t_{LH} remain zero because a plane of symmetry running through the long axis of the molecule (xy plane; see Figure 1) is preserved during vibration. On the other hand, A_2 and B_2 motions do impact these nonhorizontal terms and orbital phase plays a particularly interesting role in this context. For B_2 motions, the coupling gradients dt_{HL}/dq_i and dt_{LH}/dq_i have a common sign whereas for A_2 motions the signs are opposite. These patterns ultimately highlight whether SF pathways through two different virtual CT states (^{1}AC versus ^{1}CA) interfere destructively (B_2) or constructively (A_2). Ultimately, although this point is somewhat nuanced by coupling gradient magnitudes, A_2 motions are found to play a more prominent mechanistic role in BT1 due to this quantum interference phenomenon.

We have identified three normal modes in BT1 with the highest impact on electronic coupling for SF: mode 6 at 113.5 cm^{-1} (A_2), mode 158 at 1765 cm^{-1} (A_2), and mode 159 at 1772 cm^{-1} (B_2). Mode 6 does not stand out in the magnitude of its gradients dt_{HL}/dq_i and dt_{LH}/dq_i. Rather, it achieves prominence due to constructive interference of CT pathways as well as its low frequency that enables substantial RMS

DOI: 10.1021/jp510777c
J. Phys. Chem. A 2015, 119, 299−311

deviations in position at room temperature. The two higher frequency modes 158 and 159 have insignificant RMS deviation and must exploit larger values of dt_{HL}/dq_i and dt_{LH}/dq_i made possible by motions that strongly impact the norbornyl bridge and its two proximal phenyl rings. For mode 159 (B_2), these coupling gradients are the largest we have seen but the CT pathways destructively interfere. For mode 158 (A_2) the coupling gradient magnitudes are diminished by a factor of 2.7 (relative to mode 159) but the system can take advantage of the constructive interference.

Finally, by application of a model Hamiltonian[76] that incorporates our coupling gradients, we can back out a range of effective coupling magnitudes $|V|$ for SF as a function of possible values of the reorganization energy (λ) of the SF reaction in BT1 at room temperature. For values of λ that range from 100 meV (expected to be relevant for crystalline systems[27]) to 1000 meV (expected to be more relevant when solvent is included), the effective coupling is robust and spans a range from ∼5.4 to ∼5.8 meV. For comparative purposes, it is worthwhile to return to the noncovalent Tc dimer in which, as discussed previously, we calculated (based on t_{HH}, t_{LL}, t_{HL}, and t_{LH}) a value for electronic coupling for SF ($S_0S_1 \rightarrow {}^1TT$) of 7.3 meV under conditions where ΔE_{CT} = 600 meV. On the one hand, this would suggest that future calculations of SF should and must investigate the possibility of non-Condon effects; fluctuations in diabatic couplings might be as large the ground-state geometry coupling itself. On the other hand, if non-Condon effects are larger in BT1 than in Tc, and we suppose that BT1 and Tc have fairly similar frequencies and reorganization energies, one might speculate that BT1 might also allow for observable SF efficiencies (e.g, the efficiency of SF in crystalline Tc is 200%). We are also intrigued going forward by the notion of using experimental protocols based on laser-pulse shaping to create nonequilibrium vibrational conditions as a means of controlling SF rates and more importantly of identifying those most strongly correlated with the photophysical mechanism. In the end, we believe the simple procedure discussed here can be used to explore and identify new dimer designs that avoid key symmetries impeding SF.

■ ASSOCIATED CONTENT

Supporting Information

Additional figures: (a) cartoon of SF pathways and relevant matrix elements, (b) frontier orbitals for the Tc monomer, (c) geometry used herein for the noncovalent Tc dimer taken from the molecular crystal structure, and (d) cartoon that explores how the coupling gradient dt_{HL}/dq_i (as opposed to dt_{LH}/dq_i) develops magnitude along normal modes 158 and 159. Additional equations that incorporate two-electron integrals are included. Additional tables: (a) coupling gradients calculated for all normal modes; (b) one-electron couplings calculated at RMS deviation at 298 K for all normal modes; (c) coupling dependence on different density functionals for BT1 and non-covalent dimer; (d) coupling gradients as a function of finite difference step size; and (e) molecular orbital energy gradients. This material is available free of charge via the Internet at http://pubs.acs.org.

■ AUTHOR INFORMATION

Corresponding Author

*E-mail: Niels.Damrauer@colorado.edu.

Notes

The authors declare no competing financial interest.

■ ACKNOWLEDGMENTS

N.H.D. gratefully acknowledges support from the Chemical Sciences, Geosciences, and Biosciences Division, Office of Basic Energy Science, U.S. Department of Energy, through Grant DE-FG02-07ER15890. N.H.D. would like to thank Dr. Timothy Berkelbach for very helpful correspondence and for calculating (and sharing) certain one-electron coupling matrix elements that we used for comparison purposes in the paper. N.H.D. would also like to thank Dr. Shane Parker for very helpful correspondence and for sharing certain unpublished diabatic state couplings cast in a Frenkel exciton basis and Prof. Joel Eaves for helpful discussions regarding eqs 10 and 11. J.E.S. thanks Seogjoo Jang for very interesting discussions and acknowledges support from NSF CAREER Grant CHE-1150851 and a David & Lucile Packard Fellowship.

■ REFERENCES

(1) Green, M. *Third Generation Photovoltaics: Advanced Solar Energy Conversion*; Springer-Verlag: Berlin, 2003.
(2) Smith, M. B.; Michl, J. Singlet Fission. *Chem. Rev.* **2010**, *110*, 6891−6936.
(3) Smith, M. B.; Michl, J. Recent Advances in Singlet Fission. *Annu. Rev. Phys. Chem.* **2013**, *64*, 361−386.
(4) Shockley, W.; Queisser, H. Detailed Balance Limit of Efficiency of p-n Junction Solar Cells. *J. Appl. Phys.* **1961**, *32*, 510−519.
(5) Hanna, M. C.; Nozik, A. J. Solar Conversion Efficiency of Photovoltaic and Photoelectrolysis Cells with Carrier Multiplication Absorbers. *J. Appl. Phys.* **2006**, *100*, 074510.
(6) Burdett, J. J.; Bardeen, C. J. The Dynamics of Singlet Fission in Crystalline Tetracene and Covalent Analogs. *Acc. Chem. Res.* **2013**, *46*, 1312−1320.
(7) Roberts, S. T.; McAnally, R. E.; Mastron, J. N.; Webber, D. H.; Whited, M. T.; Brutchey, R. L.; Thompson, M. E.; Bradforth, S. E. Efficient Singlet Fission Discovered in a Disordered Acene Film. *J. Am. Chem. Soc.* **2012**, *134*, 6388−6400.
(8) Walker, B. J.; Musser, A. J.; Beljonne, D.; Friend, R. H. Singlet Exciton Fission in Solution. *Nat. Chem.* **2013**, *5*, 1019−1024.
(9) Busby, E.; Berkelbach, T. C.; Kumar, B.; Chernikov, A.; Zhong, Y.; Hlaing, H.; Zhu, X. Y.; Heinz, T. F.; Hybertsen, M. S.; Sfeir, M. Y.; et al. Multiphonon Relaxation Slows Singlet Fission in Crystalline Hexacene. *J. Am. Chem. Soc.* **2014**, *136*, 10654−10660.
(10) Kolata, K.; Breuer, T.; Witte, G.; Chatterjee, S. Molecular Packing Determines Singlet Exciton Fission in Organic Semiconductors. *ACS Nano* **2014**, *8*, 7377−7383.
(11) Wilson, M. W.; Rao, A.; Ehrler, B.; Friend, R. H. Singlet Exciton Fission in Polycrystalline Pentacene: From Photophysics toward Devices. *Acc. Chem. Res.* **2013**, *46*, 1330−1338.
(12) Mastron, J. N.; Roberts, S. T.; McAnally, R. E.; Thompson, M. E.; Bradforth, S. E. Aqueous Colloidal Acene Nanoparticles: A New Platform for Studying Singlet Fission. *J. Phys. Chem. B* **2013**, *117*, 15519−15526.
(13) Lee, J.; Bruzek, M. J.; Thompson, N. J.; Sfeir, M. Y.; Anthony, J. E.; Baldo, M. A. Singlet Exciton Fission in a Hexacene Derivative. *Adv. Mater.* **2013**, *25*, 1445−1448.
(14) Johnson, J. C.; Nozik, A. J.; Michl, J. High Triplet Yield from Singlet Fission in a Thin Film of 1,3-Diphenylisobenzofuran. *J. Am. Chem. Soc.* **2010**, *132*, 16302−16303.
(15) Schrauben, J. N.; Ryerson, J. L.; Michl, J.; Johnson, J. C. Mechanism of Singlet Fission in Thin Films of 1,3-Diphenylisobenzofuran. *J. Am. Chem. Soc.* **2014**, *136*, 7363−7373.
(16) Johnson, J. C.; Nozik, A. J.; Michl, J. The Role of Chromophore Coupling in Singlet Fission. *Acc. Chem. Res.* **2013**, *46*, 1290−1299.
(17) Ryerson, J. L.; Schrauben, J. N.; Ferguson, A. J.; Sahoo, S. C.; Naumov, P.; Havlas, Z.; Michl, J.; Nozik, A. J.; Johnson, J. C. Two

DOI: 10.1021/jp510777c
J. Phys. Chem. A 2015, 119, 299−311

Thin Film Polymorphs of the Singlet Fission Compound 1,3-Diphenylisobenzofuran. *J. Phys. Chem. C* **2014**, *118*, 12121−12132.
(18) Wang, C.; Tauber, M. J. High-Yield Singlet Fission in a Zeaxanthin Aggregate Observed By Picosecond Resonance Raman Spectroscopy. *J. Am. Chem. Soc.* **2010**, *132*, 13988−13991.
(19) Dillon, R. J.; Piland, G. B.; Bardeen, C. J. Different Rates of Singlet Fission in Monoclinic Versus Orthorhombic Crystal Forms of Diphenylhexatriene. *J. Am. Chem. Soc.* **2013**, *135*, 17278−17281.
(20) Eaton, S. W.; Shoer, L. E.; Karlen, S. D.; Dyar, S. M.; Margulies, E. A.; Veldkamp, B. S.; Ramanan, C.; Hartzler, D. A.; Savikhin, S.; Marks, T. J.; et al. Singlet Exciton Fission in Polycrystalline Thin Films of a Slip-Stacked Perylenediimide. *J. Am. Chem. Soc.* **2013**, *135*, 14701−14712.
(21) Congreve, D. N.; Lee, J. Y.; Thompson, N. J.; Hontz, E.; Yost, S. R.; Reusswig, P. D.; Bahlke, M. E.; Reineke, S.; Van Voorhis, T.; Baldo, M. A. External Quantum Efficiency Above 100% in a Singlet-Exciton-Fission-Based Organic Photovoltaic Cell. *Science* **2013**, *340*, 334−337.
(22) Lee, J.; Jadhav, P.; Reusswig, P. D.; Yost, S. R.; Thompson, N. J.; Congreve, D. N.; Hontz, E.; Van Voorhis, T.; Baldo, M. A. Singlet Exciton Fission Photovoltaics. *Acc. Chem. Res.* **2013**, *46*, 1300−1311.
(23) Berkelbach, T. C.; Hybertsen, M. S.; Reichman, D. R. Microscopic Theory of Singlet Exciton Fission. I. General Formulation. *J. Chem. Phys.* **2013**, *138*, 114102.
(24) Berkelbach, T. C.; Hybertsen, M. S.; Reichman, D. R. Microscopic Theory of Singlet Exciton Fission. II. Application To Pentacene Dimers and the Role of Superexchange. *J. Chem. Phys.* **2013**, *138*, 114103.
(25) Teichen, P. E.; Eaves, J. D. A Microscopic Model of Singlet Fission. *J. Phys. Chem. B* **2012**, *116*, 11473−11481.
(26) Parker, S. M.; Seideman, T.; Ratner, M. A.; Shiozaki, T. Model Hamiltonian Analysis of Singlet Fission from First Principles. *J. Phys. Chem. C* **2014**, *118*, 12700−12705.
(27) Yost, S. R.; Lee, J.; Wilson, M. W. B.; Wu, T.; McMahon, D. P.; Parkhurst, R. R.; Thompson, N. J.; Congreve, D. N.; Rao, A.; Johnson, K.; et al. A Transferable Model for Singlet-Fission Kinetics. *Nat. Chem.* **2014**, *6*, 492−497.
(28) Havenith, R. W. A.; de Gier, H. D.; Broer, R. Explorative Computational Study of the Singlet Fission Process. *Mol. Phys.* **2012**, *110*, 2445−2454.
(29) Beljonne, D.; Yamagata, H.; Bredas, J. L.; Spano, F. C.; Olivier, Y. Charge-Transfer Excitations Steer the Davydov Splitting and Mediate Singlet Exciton Fission in Pentacene. *Phys. Rev. Lett.* **2013**, *110*, 226402.
(30) Zeng, T.; Hoffmann, R.; Ananth, N. The Low-Lying Electronic States of Pentacene and Their Roles in Singlet Fission. *J. Am. Chem. Soc.* **2014**, *136*, 5755−5764.
(31) Casanova, D. Electronic Structure Study of Singlet Fission in Tetracene Derivatives. *J. Chem. Theory Comput.* **2014**, *10*, 324−334.
(32) Mirjani, F.; Renaud, N.; Gorczak, N.; Grozema, F. C. Theoretical Investigation of Singlet Fission in Molecular Dimers: The Role of Charge Transfer States and Quantum Interference. *J. Phys. Chem. C* **2014**, *118*, 14192−14199.
(33) Zimmerman, P. M.; Musgrave, C. B.; Head-Gordon, M. A Correlated Electron View of Singlet Fission. *Acc. Chem. Res.* **2013**, *46*, 1339−1347.
(34) Akimov, A. V.; Prezhdo, O. V. Nonadiabatic Dynamics of Charge Transfer and Singlet Fission at the Pentacene/C60 Interface. *J. Am. Chem. Soc.* **2014**, *136*, 1599−1608.
(35) Chan, W. L.; Berkelbach, T. C.; Provorse, M. R.; Monahan, N. R.; Tritsch, J. R.; Hybertsen, M. S.; Reichman, D. R.; Gao, J. L.; Zhu, X. Y. The Quantum Coherent Mechanism for Singlet Fission: Experiment and Theory. *Acc. Chem. Res.* **2013**, *46*, 1321−1329.
(36) Renaud, N.; Sherratt, P. A.; Ratner, M. A. Mapping the Relation between Stacking Geometries and Singlet Fission Yield in a Class of Organic Crystals. *J. Phys. Chem. Lett.* **2013**, *4*, 1065−1069.
(37) Feng, X. T.; Luzanov, A. V.; Krylov, A. I. Fission of Entangled Spins: An Electronic Structure Perspective. *J. Phys. Chem. Lett.* **2013**, *4*, 3845−3852.
(38) Zeng, T.; Ananth, N.; Hoffmann, R. Seeking Small Molecules for Singlet Fission: A Heteroatom Substitution Strategy. *J. Am. Chem. Soc.* **2014**, *136*, 12638−12647.
(39) Müller, A. M.; Avlasevich, Y. S.; Schoeller, W. W.; Müllen, K.; Bardeen, C. J. Exciton Fission and Fusion in Bis(Tetracene) Molecules with Different Covalent Linker Structures. *J. Am. Chem. Soc.* **2007**, *129*, 14240−14250.
(40) Havlas, Z.; Michl, J. Unpublished calculations.
(41) Vallett, P. J.; Snyder, J. L.; Damrauer, N. H. Tunable Electronic Coupling and Driving Force in Structurally Well-Defined Tetracene Dimers for Molecular Singlet Fission: A Computational Exploration Using Density Functional Theory. *J. Phys. Chem. A* **2013**, *117*, 10824−10838.
(42) Wang, L.; Olivier, Y.; Prezhdo, O.; Beljonne, D. Maximizing Singlet Fission by Intermolecular Packing. *J. Phys. Chem. Lett.* **2014**, *5*, 3345−3353.
(43) Greyson, E. C.; Vura-Weis, J.; Michl, J.; Ratner, M. A. Maximizing Singlet Fission in Organic Dimers: Theoretical Investigation of Triplet Yield in the Regime of Localized Excitation and Fast Coherent Electron Transfer. *J. Phys. Chem. B* **2010**, *114*, 14168−14177.
(44) Berkelbach, T. C.; Hybertsen, M. S.; Reichman, D. R. Microscopic Theory of Singlet Exciton Fission. III. Crystalline Pentacene. *J. Chem. Phys.* **2014**, *141*, 074705.
(45) Kuhlman, T. S.; Kongsted, J.; Mikkelsen, K. V.; Møller, K. B.; Sølling, T. I. Interpretation of the Ultrafast Photoinduced Processes in Pentacene Thin Films. *J. Am. Chem. Soc.* **2010**, *132*, 3431−3439.
(46) Zimmerman, P. M.; Bell, F.; Casanova, D.; Head-Gordon, M. Mechanism for Singlet Fission in Pentacene and Tetracene: From Single Exciton to Two Triplets. *J. Am. Chem. Soc.* **2011**, *133*, 19944−19952.
(47) Zimmerman, P. M.; Zhang, Z.; Musgrave, C. B. Singlet Fission in Pentacene through Multi-Exciton Quantum States. *Nat. Chem.* **2010**, *2*, 648−652.
(48) Grumstrup, E. M.; Johnson, J. C.; Damrauer, N. H. Enhanced Triplet Formation in Polycrystalline Tetracene Films By Femtosecond Optical-Pulse Shaping. *Phys. Rev. Lett.* **2010**, *105*, 257403.
(49) Interestingly, this work as well as the work mentioned above by Zimmerman and co-workers (cf. ref 46) is at odds with interpretations of temperature-independent spectroscopic data (cf. refs 50−52) where, for example based on transient absorption studies, it has been suggested that SF in Tc occurs between isoenergetic reactant and product states via vibronic tunneling in the limit of small electronic coupling (cf. ref 50). We will not consider such vibronic tunneling here, but in this context intermolecular motions might play some role mediating a tunneling barrier.
(50) Wilson, M. W. B.; Rao, A.; Johnson, K.; Gelinas, S.; di Pietro, R.; Clark, J.; Friend, R. H. Temperature-Independent Singlet Exciton Fission in Tetracene. *J. Am. Chem. Soc.* **2013**, *135*, 16680−16688.
(51) Burdett, J. J.; Gosztola, D.; Bardeen, C. J. The Dependence of Singlet Exciton Relaxation on Excitation Density and Temperature in Polycrystalline Tetracene Thin Films: Kinetic Evidence for a Dark Intermediate State and Implications for Singlet Fission. *J. Chem. Phys.* **2011**, *135*, 214508.
(52) Tayebjee, M. J. Y.; Clady, R. G. C. R.; Schmidt, T. W. The Exciton Dynamics in Tetracene Thin Films. *Phys. Chem. Chem. Phys.* **2013**, *15*, 14797−14805.
(53) Johnson, J. C.; Akdag, A.; Zamadar, M.; Chen, X.; Schwerin, A. F.; Paci, I.; Smith, M. B.; Havlas, Z.; Miller, J. R.; Ratner, M. A.; et al. Toward Designed Singlet Fission: Solution Photophysics of Two Indirectly Coupled Covalent Dimers of 1,3-Diphenylisobenzofuran. *J. Phys. Chem. B* **2013**, *117*, 4680−4695.
(54) Scholes, G. D.; Ghiggino, K. P.; Oliver, A. M.; Paddon-Row, M. N. Through-Space and Through-Bond Effects on Exciton Interactions in Rigidly Linked Dinaphthyl Molecules. *J. Am. Chem. Soc.* **1993**, *115*, 4345−4349.
(55) The notation that is used here for diabatic states relates to the monomer units A and B in that order. So, for example, S_1S_0 means that unit A is in the first excited singlet state while B is in the ground state.

DOI: 10.1021/jp510777c
J. Phys. Chem. A 2015, 119, 299−311

As a further example, ^{1}CA means that monomer A is oxidized (cationic) while monomer B is reduced (anionic).
(56) Of course, such an orbital description ignores any and all effects of electron correlation so that, for accuracy, this approach will necessary rely on a fortuitous cancellation of errors—which holds quite often.
(57) Shao, Y.; Molnar, L. F.; Jung, Y.; Kussmann, J.; Ochsenfeld, C.; Brown, S. T.; Gilbert, A. T. B.; Slipchenko, L. V.; Levchenko, S. V.; ONeill, D. P.; et al. Advances in Methods and Algorithms in a Modern Quantum Chemistry Program Package. *Phys. Chem. Chem. Phys.* **2006**, *8*, 3172−3191.
(58) Krylov, A. I.; Gill, P. M. W. Q-Chem: An Engine for Innovation. *Wiley Interdiscip. Rev.: Comput. Mol. Sci.* **2013**, *3*, 317−326.
(59) Chai, J. D.; Head-Gordon, M. Long-Range Corrected Hybrid Density Functionals with Damped Atom-Atom Dispersion Corrections. *Phys. Chem. Chem. Phys.* **2008**, *10*, 6615−6620.
(60) Boys, S. F. Construction of Some Molecular Orbitals to Be Approximately Invariant for Changes from One Molecule to Another. *Rev. Mod. Phys.* **1960**, *32*, 296−299.
(61) Foster, J. M.; Boys, S. F. Canonical Configurational Interaction Procedure. *Rev. Mod. Phys.* **1960**, *32*, 300−302.
(62) Edmiston, C.; Ruedenberg, K. Localized Atomic and Molecular Orbitals. *Rev. Mod. Phys.* **1963**, *35*, 457−465.
(63) Paddon-Row, M. N.; Wong, S. S. A Correlation between the Rates of Photoinduced Long-Range Intramolecular Electron-Transfer in Rigidly Linked Donor-Acceptor Systems and Computed π, π and π^*, π^* Splitting Energies in Structurally Related Dienes. *Chem. Phys. Lett.* **1990**, *167*, 432−438.
(64) Jordan, K. D.; Paddon-Row, M. N. Analysis of the Interactions Responsible for Long-Range through-Bond-Mediated Electronic Coupling between Remote Chromophores Attached to Rigid Polynorbornyl Bridges. *Chem. Rev.* **1992**, *92*, 395−410.
(65) Hanwell, M. D.; Curtis, D. E.; Lonie, D. C.; Vandermeersch, T.; Zurek, E.; Hutchison, G. R. Avogadro: An Advanced Semantic Chemical Editor, Visualization, and Analysis Platform. *J. Cheminf.* **2012**, *4*17.
(66) Cave, R. J.; Newton, M. D. Generalization of the Mulliken-Hush Treatment for the Calculation of Electron Transfer Matrix Elements. *Chem. Phys. Lett.* **1996**, *249*, 15−19.
(67) Holmes, D.; Kumaraswamy, S.; Matzger, A. J.; Vollhardt, K. P. C. On the Nature of Nonplanarity in the [N]Phenylenes. *Chem.—Eur. J.* **1999**, *5*, 3399−3412.
(68) These calcluations pertaining to the noncovalent Tc dimer that were made using the BHR-HF method were generously provided to us by Dr. T. Berkelbach.
(69) Kistler, K. A.; Spano, F. C.; Matsika, S. A Benchmark of Excitonic Couplings Derived from Atomic Transition Charges. *J. Phys. Chem. B* **2013**, *117*, 2032−2044.
(70) Sebastian, L.; Weiser, G.; Bassler, H. Charge Transfer Transitions in Solid Tetracene and Pentacene Studied By Electroabsorption. *Chem. Phys.* **1981**, *61*, 125−135.
(71) Burdett, J. J.; Muller, A. M.; Gosztola, D.; Bardeen, C. J. Excited State Dynamics in Solid and Monomeric Tetracene: The Roles of Superradiance and Exciton Fission. *J. Chem. Phys.* **2010**, *133*, 144506.
(72) Longuet-Higgins, H. C.; Roberts, M. d. V. The Electronic Structure of the Borides MB_6. *Proc. R. Soc. London, Ser. A: Math. Phys. Eng. Sci.* **1954**, *224*, 336−347.
(73) Mulliken, R. S. The Theory of Molecular Orbitals. *J. Chim. Phys. Phys.-Chim. Biol.* **1949**, *46*, 497−542.
(74) Ayed, O.; Bernard, E.; Silvi, B. On the Mulliken Approximations of Multicentre Integrals. *J. Mol. Struct.: THEOCHEM* **1986**, *135*, 159−168.
(75) Jortner, J.; Rice, S. A.; Katz, J. L. Triplet Excitons in Crystals of Aromatic Molecules. *J. Chem. Phys.* **1965**, *42*, 309−323.
(76) Medvedev, E. S.; Stuchebrukhov, A. A. Inelastic Tunneling in Long-Distance Biological Electron Transfer Reactions. *J. Chem. Phys.* **1997**, *107*, 3821−3831.
(77) It would be interesting to construct an effective coupling through more rigorous rate theories for singlet fission, e.g., cf. ref 25.

NOTE ADDED AFTER ASAP PUBLICATION

This article posted asap on December 31, 2014. Equations 7 and 21 along with the first sentence that immediately follows these equations have been revised. The correct version posted on December 31, 2014.

DOI: 10.1021/jp510777c
J. Phys. Chem. A 2015, 119, 299−311